Received: 30 July 2020 | Revised: 26 February 2021 | Accepted: 26 March 2021

DOI: 10.1002/rcs.2257

ORIGINAL ARTICLE

The International Journal of Medical Robotics and Computer Assisted Surgery

WILEY

Development and in vivo assessment of a novel MRI-compatible headframe system for the ovine animal model

Marco Trovatelli[1] | Stefano Brizzola[1] | Davide Danilo Zani[1] | Antonella Castellano[2] | Paola Mangili[3] | Marco Riva[4] | Max Woolley[5] | Dave Johnson[5] | Ferdinando Rodriguez y Baena[6] | Lorenzo Bello[4] | Andrea Falini[2] | Riccardo Secoli[6]

[1]Department of Veterinary Medicine, Universitá degli Studi di Milano, Milan, Italy

[2]Neuroradiology Unit and C.E.R.M.A.C., Vita-Salute San Raffaele University and IRCCS Ospedale San Raffaele, Milan, Italy

[3]Medical Physics Unit, Vita-Salute San Raffaele University and IRCCS Ospedale San Raffaele, Milan, Italy

[4]Department of Oncology and Hematology-Oncology, Universitá degli Studi di Milano, Milan, Italy

[5]Renishaw Neuro Solutions Ltd., Wotton-Under-Edge, UK

[6]The Mechatronics in Medicine Laboratory, Department of Mechanical Engineering, Imperial College London, London, UK

Correspondence

Riccardo Secoli, The Mechatronics in Medicine Laboratory, Department of Mechanical Engineering, Imperial College London, London, UK.
Email: r.secoli@imperial.ac.uk

Funding information

European Union's EU Research and Innovation Programme Horizon 2020, Grant/Award Number: 688279

Abstract

Background: The brain of sheep has primarily been used in neuroscience as an animal model because of its similarity to the human brain, in particular if compared to other models such as the lissencephalic rodent brain. Their brain size also makes sheep an ideal model for the development of neurosurgical techniques using conventional clinical CT/MRI scanners and stereotactic systems for neurosurgery.

Methods: In this study, we present the design and validation of a new CT/MRI compatible head frame for the ovine model and software, with its assessment under two real clinical scenarios.

Results: Ex-vivo and in vivo trial results report an average linear displacement of the ovine head frame during conventional surgical procedures of 0.81 mm for ex-vivo trials and 0.68 mm for in vivo tests, respectively.

Conclusions: These trial results demonstrate the robustness of the head frame system and its suitability to be employed within a real clinical setting.

KEYWORDS

animal model, invivo trial, MR-compatible headframe, neurosurgery, ovine model

1 | INTRODUCTION

Over the past three decades, translational biomedical researches have seen the use of ovine models for different applications, ranging from orthopedics,[1] traumatic brain injury studies[2] and neurological diseases,[3] to more specific studies such for Alzheimer's disease[4] and epilepsy.[5] Both the large size of the ovine brain as well as anatomical features of the skull mean the ovine model is an ideal candidate in conventional stereotactic techniques for deep brain stimulation, as shown by Stypulkowski et al. for the thalamus,[6] and more recently, on the hippocampus.[7] Stereotactic methods have been widely used in other large animal models such as the pig. For instance,

Bjarkam et al.[8] developed a stereotactic procedure which enables MRI guided isocentric stereotaxy, and White et al.[9] established a method for stereotactic delivery of catheters and electrodes for reaching deep targets in the brain. Stereotactic procedures have been developed even in sheep for neurosurgical purposes, such as in Oheim et al.[10] for the intra-cerebroventricular application of leptin into the lateral ventricle. The stereotactic surgical approach has also been used for continuous monitoring of the electroencephalographic activity through the insertion of needles, as shown by Perentos et al.[11] Despite these studies, to our knowledge, only a few stereotactic head frames were shown to be compatible with the conventional Cosman Roberts Wells (CRW) Stereotactic System©. Most of the head frames were employed in studies with pig models,[9,12,13] with a design that could not easily be scaled to the ovine model, and was not suitable for clinical use, as reported by Oheim et al.[10]

The present work focuses on the design of a new head frame system (HFS) for the ovine model, suitable for MRI and CT studies, designed to work with more widely available CRW Stereotactic System©. The new HFS was developed following clinical requirements for neurosurgical applications. The work presents the validation of the HFS under a real clinical setting, firstly with an assessment ex-vivo and subsequently, during in vivo trials.

2 | MATERIALS AND METHODS

2.1 | Head frame system: requirements

The following main design requirements were deemed necessary for the HFS to perform safely and correctly under a real clinical setting:

1. to be compatible and safe for use within a magnetic resonance imaging (MRI) system.
2. to be suitable for use within a computerized tomography (CT) scanner.
3. with a footprint small enough to fit within the bore of a conventional MRI unit.
4. with a structure capable of being fixed firmly on a stretcher for easy transportation.
5. with a head fixation system capable of withstanding forces and torques caused by the motion of the body of the animal during sedation, neurosurgical procedures and transportation.
6. with a design capable of following conventional clinical procedures during general anaesthesia such as blood sampling, mucosa checking and nasogastric tube introduction.

2.2 | Head frame system: design

The HFS represented in Figures 1 and 2 was designed to clamp an ovine head to a Cosman-Roberts-Wells (CRW) stereotactic frame. The ovine head frame weights 525 kg, with a measured footprint of 360 × 350 mm, and can accommodate an ovine head within a workspace of 180 × 280 mm. As shown in the highlight ⑥ of Figure 2, clamping is achieved through the tightening of two opposing head pins onto the zygomatic arches of the ovine skull. Additional rotational support is provided by a mouth clamp (⑦ in Figure 2), which bonds the upper pallet and nose arch. The system has been designed with adjustable headpins and a mouth clamp to accommodate a range of different head sizes without impacting on the rigidity of the fixturing. Interchangeable support pillars allow an adjustable height between the u-frame and the support base. These features enable the ovine head to be placed in the isocentre of the MRI scanning volume, while still ensuring patient airways remain clear. Frame-based stereotactic procedures are facilitated through CRW arc systems that can be clamped into the novel frame using the same kinematic interface present on CRW's universal compact head rings. The relative position between the kinematics and head pins has been designed to align the brain of the ovine head in the centre of the working volume of a CRW frame.

A removable bespoke localiser arch ⑤ featuring seven fiducial spheres is used to co-register the coordinate system of the MRI or CT scanner with the coordinate system of the CRW stereotactic frame. The fiducial spheres are aligned with the ovine head to ensure proper distribution over the ovine brain.

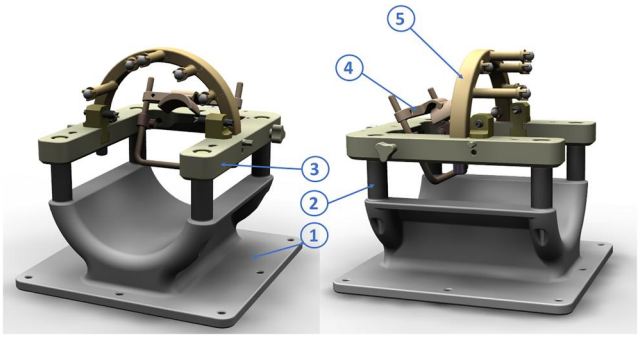

FIGURE 1 Rendering of the new head frame system with arc fiducials for MR/CT registrations

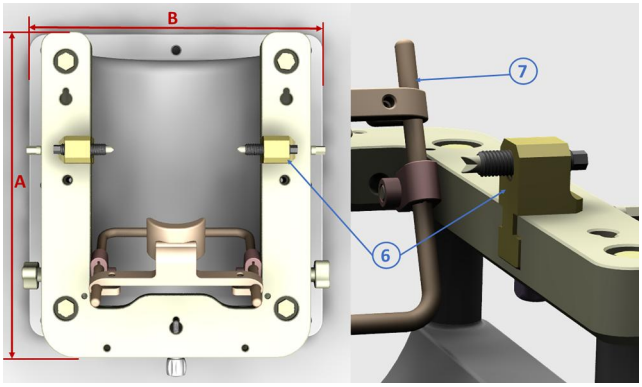

FIGURE 2 Render top view of the new head frame system with highlight of ovine head pins. Head frame footprint of (A) 360 mm and (B) 350 mm

2.3 | Head frame system: ex-vivo validation

A set of ex-vivo trials, and subsequently in vivo trials following the 3R rules,[14] were performed to assess the HFS under a real clinical setting. Four additional spherical radiopaque markers 8 mm in diameter (BrainLab AG, Germany), fixed by titanium screws onto the skull, were used to assess any possible motion of the ovine head during all of the different phases (sedation, transportation, surgery). These four additional markers were screwed randomly in four anatomical areas (one marker per area): on the frontal bone, on the occipital bone, on the anterior orbits bone and on the posterior dorsal orbits bone, as shown in Figures 3–5. For both sets of trials, pre-and post-operative CT imaging sequences were acquired with a clinical system (GE Healthcare CT system, 16 slices helical scan). The imaging sequences were acquired with standard display field of view (DFOV), matrix of 512 × 512, slice thickness of 0, 625 mm, 120 kilovolt (KV), 220 milliampere (mA), pitch 0, 562 : 1 and 1/s tube rotation. The images were collected using a soft tissue algorithm provided within the software of the scanner.

2.3.1 | Ex-vivo trials

Eight female adults, 70 kg, *Ovis aries* sheep *Bergamasca* heads were used for the assessment of the HFS in the ex-vivo test. Each ovine head was comprehensive of the neck up to the C3 vertebra.

Head fixation

As per HFS design features, the sheep head was fixed using two pins clamped against the zygoma bone, without any skin incisions. The mouth bar was placed under the hard palate and the nose clamp was pressed against the nasal bone. To replicate the sheep's body, a foam box was placed underneath the neck and secured to the HFS via velcro straps. The HFS was connected to a medical spinal stretcher (MRI and CT compatible) via plastic zip ties as in Figure 4.

Planning software and registration

A conventional neurosurgical procedure which sees the insertion of a straight, rigid needle to reach a predefined target (e.g. a deep lesion) was used as a mock of the real clinical scenario of catheter planning and procedure. The target location was identified by the surgeon

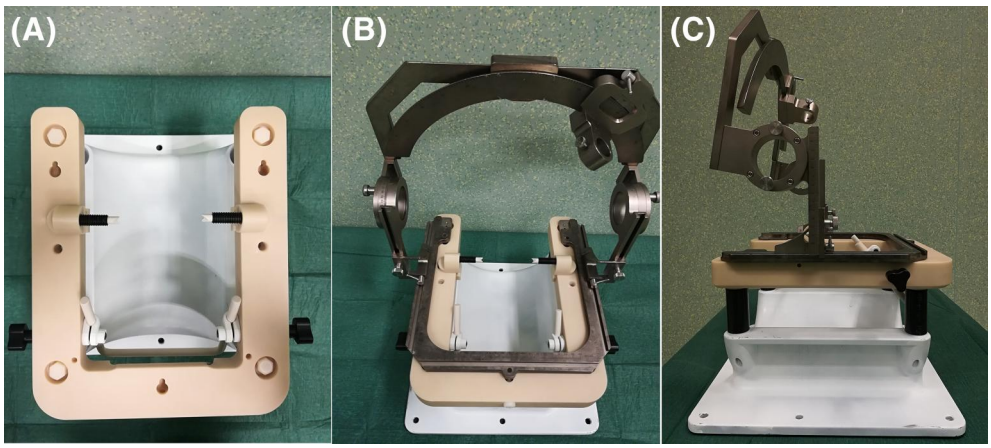

FIGURE 3 (A) top view of the head frame showing the head pins and mouth guard to fix the ovine head. Top view shown the three connection point for the CRW frame as well as the two connection point for the localiser arch. (B and C) Front and side view of a CRW system mounted on the head frame

FIGURE 4 Positioning of the ovine with head frame

from an Atlas of the ovine white matter bundle,[15] establishing the point in the corticospinal tract. The surgical procedure started with a pre-operative CT scan after the ovine head was fixed onto the Head Frame as described in the previous section. The needle trajectories were planned using a bespoke version of the commercial neurosurgical software neuroinspire™ (Renishaw inc.), which original version is designed to work in conjunction with the neurosurgical robot, the neuromate™ – (Renishaw plc). In this version, the software has been designed to work in conjunction with Cosman-Roberts-Wells (CRW) stereotactic frame, widely used in neurosurgical applications. The

FIGURE 5 Ex-vivo surgical scenario after burr hole drilling. In the picture are noted three of the four fiducial spheres

facto, this combination provide a certified planning software for medical used into preclinical studies uses. The software uses 7 fiducials spread along a removable circular arc used to register the HFS with the CRW frame. As shown in Figure 6, the front-end interface provides the CT image of the head frame with a widget showing the displacement of the fiducials within the arc. The user registers each fiducial by selecting each one by one on the top-left widget. Once a fiducial is selected, a circular marker appears on the medical image in correspondence with the position estimate of the selected fiducial on the medical image. In a subsequent step, the user refines the position of the circular marker on the medical image, by moving it using orthogonal zoomed views, as shown on the right widget of Figure 6. Once registration of all seven markers is complete, further registration of different image modalities can be performed automatically by the software. In the example shown in Figure 7, a standard stereotactic ovine MRI reference template[16] was registered to the CT scan, and a Diffusion Tensor Imaging MR tractography reconstruction of the ovine corticospinal tracts was integrated in the planning,[15] as part of the multi-modal planning tools exploited in the EDEN2020 project (www.eden2020.eu). As targets, one point for each corticospinal tract (two targets per trial) was selected. In a final step, the user planned suitable trajectories for the tool by selecting the entry point location on the skull and the target location according to a given clinical case. An example is shown in Figure 7.

The area of surgical access was identified approximately 15 mm cranially to the coronal suture line and roughly 10 mm laterally to the metopic suture line. Ideally, the entry point area had a flat surface above the corticospinal tracts in a zone which was free from

FIGURE 6 Screenshot of the neuroinspire™, Renishaw inc – registration arc-fiductials of the HFS with the CRW frame

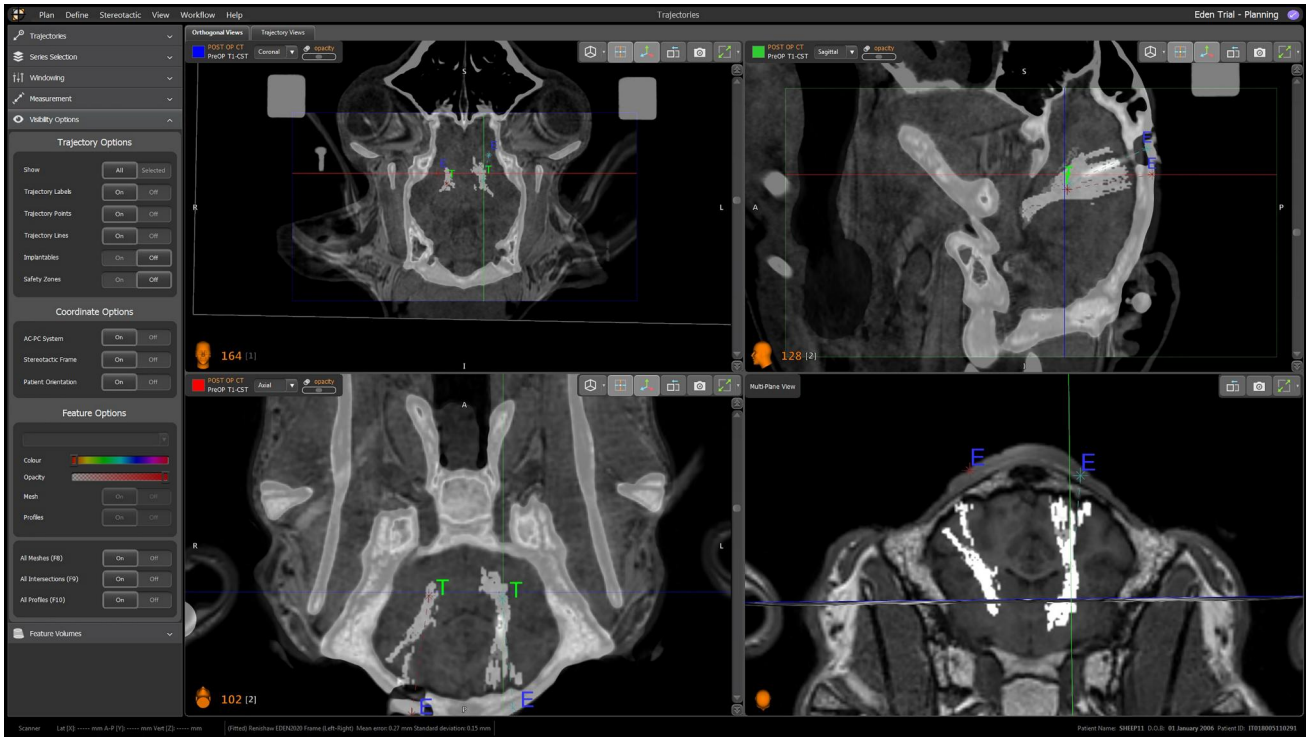

FIGURE 7 Screenshot of the neuroinspire™, Renishaw inc – during the planning of rigid catheter insertion

significant vessels. Once the area was identified and selected on the software, a set of coordinates on the CRW stereotactic system were provided. The CRW was then assembled on the top plate of the HFS, and a verification shaft tool was used to match the entry point shown in the software. Once the entry point was verified, it was marked on the skull using a pencil to facilitate the drilling phase. This work aims to demonstrate the head frame's performance, measured as the ability to lock in position an ovine head model during two clinical scenarios. To achieve this purpose, we have used the bigger drill size for a neurosurgical procedure to exert the maximum stress on the skull, thus the drilling was performed using a conventional neurosurgical perforator 14 mm in diameter (CODMAN® Disposable Perforator 14 mm – Drill: ANSPACH® EMAX® 2 Plus System by DePuy Synthes). Following the neurosurgical procedure, the HFS was moved to the CT scanner for postoperative image acquisition. The data acquired were analysed to measure any head displacement after initial placement and first CT scanning.

2.4 | In vivo trials

After a clinical evaluation of the HFS using ex-vivo samples, the HFS was validated in vivo. All animals were treated under the European Communities Council Directive (2010/63/EU), adhering to the laws and regulations on animal welfare enclosed in D.L.G.S. 26/2014 and approved by the Italian Health Department with authorization n° 635/2017.

2.4.1 | Animal anaesthesia

A total of four sheep *ovis aries* (average 70 kg, all female, one year old) were used in this study. The animals were under general anaesthesia for all of the procedures described in the following sections. Animals were inducted via intravenous administration of *Diazepam* 0, 25 mg/kg + *Ketamine* 5 mg/kg, intubated and then maintained under general anaesthesia with *isoflurane* 2% and *oxygen* 2 L/m. Two peripheral venous accesses in right and left auricular veins were set for each sheep and urinary catheterization performed.

2.4.2 | In vivo procedure

The in vivo trials procedure was carried out as follow:

1. A general anaesthesia is administered to the animal, as described above.
2. The sheep is located on a spinal stretcher (acrylonitrile butadiene styrene, ABS stretcher, Millenia, Ferno) and it is secured in a prone position on a vacuum mattress with extended legs, via two straps.
3. The HFS is placed onto the stretcher and secured using a bespoke fixture system.
4. The animal head is fixed into the HFS and additional fiducial markers mounted in the same anatomical areas as in the ex-vivo trials.

5. Acquisition of the first CT imaging sequence (CT-pre) at facility A.
6. Acquisition of a pre-operative MRI volume at facility B.
7. The sheep undergoes the surgical procedure (auth n° 635/2017) at facility A.
8. A second CT imaging sequence is recorded (post-CT) at facility A.

3 | RESULTS

3.1 | Image analysis for linear motion of the ovine head

The following imaging process was carried out using 3DSlicer,[17] while the assessment of the linear motion of the ovine head within the HFS during the procedures (ex-vivo and in vivo trials), expressed as the Target Registration Error of the four Additional Fiducials Marker (AFM), was carried out using bespoke software in Matlab (version 2018b, Mathworks Inc). The steps were as follows:

1. CT pre-operative (CT-pre) and post-operative sequences (CT-post) were loaded into the 3DSlicer software.
2. An intensity filter was applied to the series between W 3000 HU and WL 600 HU, range where arch fiducials of the HFS and the AFM have maximum intensity.
3. Two meshes, one for pre-operative images (PreOP-Mesh) and one for post-operative images (PostOP-Mesh), were generated.
4. PreOP-Mesh and PostOP-Mesh were registered using the Iterative Closest Point algorithm (Matlab 2018b - Mathworks Inc. - function *pcregistericp* - Tolerances: 0.01 mm translation, 0.05deg rotation, Max interaction 1000 loops) applied to the centroids of the fiducials of the Bespoke localiser (see n.5 on Table 1).
5. The output of the registration process defines a transformation matrix T.
6. The Centroids of AFMs in the PreOP and PostOP Meshes were extracted using a bespoke algorithm and identified respectively as C_{AFMpre} and $C_{AFMpost}$.
7. The transformation T was applied to each C_{AFMpre} to generate the corresponding centroid on the PostOP reference frame. These fiducials were defined as $\hat{C}_{AFMpre}$.
8. The Target Registration Error (TRE) was calculated [18] by using C_{AFMpre} and $\hat{C}_{AFMpre}$, with mean (Π) and standard deviation (σ) of TREs defined as follow.

$$\Pi = \frac{1}{4}\sum_{i=1}^{4} TRE_i \qquad (1)$$

$$\sigma = \sqrt{\frac{1}{4}\sum_{i=1}^{4}(TRE_i - \Pi)^2}$$

The results for the ex-vivo and in vivo tests are reported in Tables 2 and 3, respectively. The average linear motion for the ex-vivo trials was 0.81 ± 0.54 mm, while for the in vivo trials was 0.68 ± 0.61 mm. Rotational motion respect to the centre of rotation (CrO) identified by the intersection between the axis linking the two head pins and axis lying on the median sagittal plane of the head are considered negligible as below 1° degree (the distance between the CrO and fiducials is between around 74mm and 80mm according to sheep's head size). The average RMSE for Arc Fiducial registration Error (FRE), output of the ICP algorithm for both tests was: 0.46 ± 0.12, in line with results of previous work[9] using the software described in Section 2.3.1.

3.2 | MR performance test

The following section is divided in two parts: the first follow a clinical protocol using a ACR MR phantom to assess geometric distortions while the second part is a qualitative assessment following NEMA protocol.

TABLE 1 Parts of the Head Frame with materials used for the manufacturing

Part n.	Description	Materials
①	Support base	Nylon
②	Support pillar	Acetal
③	U-frame	PU
④	Mouth clamp	Acetal, PEEK and Nylon
⑤	Bespoke localiser	Nylon with CT/MR fiducials
⑥	Ovine head pins	PU, PEEK and acetal
⑦	As in for ④	PEEK

TABLE 2 Results of ex-vivo trials

Trial n.	Π ± σ [mm]	Arc FRE [rmse]
1	0.93 ± 0.7	0.73
2	1.07 ± 0.86	0.28
3	0.81 ± 0.45	0.55
4	1.04 ± 0.26	0.49
5	0.55 ± 0.15	0.46
6	0.95 ± 0.9	0.38
7	0.71 ± 0.05	0.29
8	0.46 ± 0.09	0.44

TABLE 3 Results of in vivo trials

Trial n.	Π ± σ [mm]	Arc FRE [rmse]
1	0.35 ± 0.13	0.53
2	0.75 ± 0.18	0.59
3	0.74 ± 0.56	0.41
4	0.83 ± 0.1	0.44

3.2.1 | ACR phantom set-up and acquisition

A small ACR MRI phantom acquisition was performed on a 1.5T clinical scanner (Achieva, Philips Healthcare) with a 60 cm bore diameter using two different settings for acquisition: with and without the head frame. Small and medium flexible surface coils were fixed over both hemispheres were wrapped around the phantom, as showed in Figures 8 and 9, in order to simulate a realistic clinical setting.[15] The ACR phantom was carefully positioned and aligned for each scan session, strictly following the ACR scanning instruction.[19] A single slice sagittal localizer, T1 and T2 ACR spin echo acquisition as well as a three-dimensional fast-field-echo (3D-T1 FFE) sequence (repetition time/echo time (TR/TE) 20 ms/3.7 ms; flip angle 40°; voxel size 0.667 × 0.667 × 1.4 mm; SENSE factor $R = 2$) according to the clinical protocol were acquired. Phantom image analysis was conducted by an MRI physicist, strictly following the ACR test guidance. Quantitative measurements included geometric accuracy, high-contrast spatial resolution, slice thickness accuracy, image intensity uniformity and percent-signal ghosting. 0 pt–5 pt.

3.2.2 | ACR test results

The two-measurement dataset (with head frame and without head frame) were statistically tested (reference $p_{value} = 0.05$) for normality with Shapiro–Wilk test (result $p_{value} > 0.1$) and then compared using a two-tailed paired *t*-test. No significant differences were found between the two datasets using ACR MRI phantom, respectively T1: $p_{value} = 0.07$ and T2: $p_{value} = 0.51$. In particular, the percentual geometric distortions calculated as the percentage difference between the measurements and the real value of ACR, were similar for both the settings and reported in Table 4 [AGGIUNGERE METODO DI CALCOLO]. The spatial resolution for both T1 and T2 images was 0.7 mm for upper-left (UL) hole arrays and 0.7 mm for lower-right (LR) hole arrays for both settings. The slice thickness measured on ACR T1 images was 4.96 mm without the head frame and 5.02 mm with the head frame. Image intensity uniformity calculated as percent integral uniformity (PIU) was 100.89 without the head frame and 100.97 with the head frame. Percent-signal ghosting ratio was 2.10% without the head frame and 0.83% with the head frame.

3.2.3 | Qualitative assessment

A further test was carried out to show a qualitative assessment of the Head Frame. Experimental condition and MR sequence were kept the same as in the ACR assessment. The prototype was installed at the centre of the field of view as shown in Figure 9, with a standard MR cylindrical phantom containing a saline solution of nickel sulphate ($N_lSO_4 + 6H_2O$/2.62g NaCl) placed inside the Head Frame. As for the ACR test, two image dataset were generated: the first dataset with only the phantom and the second dataset, with the Phantom and the Head Frame. Coronal slices were used in this evaluation. An example

FIGURE 8 In vivo clinical setting of live ovine model with the head frame system during a CT acquisition

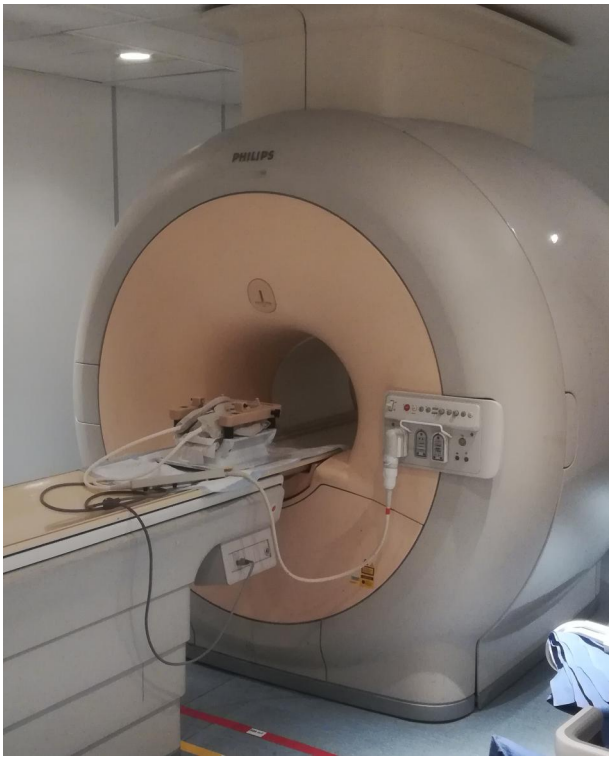

FIGURE 9 MR test setup with the Head Frame placed inside the bore of the machine during ACR test

TABLE 4 Geometric accuracy of the ACR MRI acquisition under the two settings: with and without head frame system (HFS)

	Without HFS				With HFS			
Measurement Index	**T1**	**%**	**T2**	**%**	**T1**	**%**	**T2**	**%**
Phantom length (localizer)	100.1	0.10			99.2	−0.8		
Diameter (AP direction)	100.18	0.18	99.823	−0.18	99.558	−0.44	100.7	0.70
Diameter (LR direction)	100.18	0.18	100.221	0.22	99.956	−0.04	100.2	0.20
Diameter (AP direction)	99.558	−0.44	100.7	0.70	99.558	−0.44	99.6	−0.40
Diameter (LR direction)	100.221	0.22	100.2	0.20	100.088	0.09	100.7	0.70
Diameter (phantom's UL to LR)	99.677	−0.32	100.7	0.70	99.696	−0.30	100.7	0.70
Diameter (phantom's UR to LL)	99.885	−0.11	99.8	−0.20	99.743	−0.26	100.9	0.90

Abbreviations: AP, Anterior-Posterior; LL, Lower-Left; LR, Lower-Right; UL, Upper-Left; UR, Upper-Right.

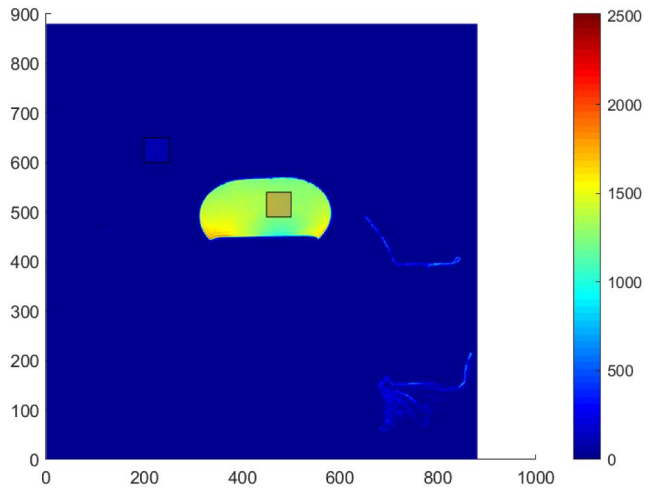

FIGURE 10 Signal-to-Noise Ratio of Slice n.20: dataset with phantom and Head Frame. Bottom-right shadows is water moist over part of the Head Frame structure

slice from the image set is reported in Figure 10: the image shows no geometrical imaging artifacts caused by the Head Frame.

Signal-to-Noise Ratio as NEMA procedure

The data analysis was carried out following the National Electrical Manufacturers Association (NEMA) procedures[20] standard assuming a statistically and spatially uniform distribution of noise. Two regions of interests (ROIs) of 50 × 50 pixels were selected as shown in Figure 10: one region inside the tissue phantom, and a second region outside the tissue phantom and far from the Head Frame. The noise was computed for all images, covering the whole footprint of the Head Frame, individually, and then averaged. The first image set, image set A (with only the phantom inside the MRI) was considered as the baseline, of which SNR is reported in Figure 11 (Top) in red. The total variation of the SNR for image set B (with Head Frame – blue line in Figure 11 (Top)) was 1255.2 (−41.9% – red line). The average SNR value for the baseline was 2160.8, which was calculated as reported in References.[21–23] A sample slice of the full imaging sequences is reported in Figure 11 Middle and Bottom, respectively, the sequence without the Head Frame and with the Head Frame.

4 | DISCUSSION

Sheep has been employed as the animal model for translational applications in a range of studies including epilepsy,[5] neuropsychiatrics,[24] traumatology,[2] cardiovascular[25] and neurological diseases.[3] The ovine brain size features gyrencephalic sulci as in the human brain, showing better modelling characteristics when compared to lissencephalic rodent brain.[26] Even if primate brains are anatomically and functionally more similar to human brains, their use is limited due to the strict ethical constraints.[27,28] The pig animal model seems to be the most used in neuroscience,[29,30] but aspects of their skull anatomy should be considered. For instance, the anterior pig head has a planar forehead and vertex that end in a high crest where the neck muscles are inserted. Laterally, the vertex is limited by the parietal bone, reducing the accessible brain area to a small square, as shown in Reference [31]. Additionally, minipig breeds and domestic pig have a fast growth index if compared with sheep, with an average daily weight gain for Large White-Landrace reported to be between 734 and 992 g/day in the first 6 months of life,[32] reaching the adult stage (1–2 years in age) at more than 300 kg.[29] Last, minipig and pig models at 3–6 months develop a sizeable frontal sinus that pneumatizes all of the dorsolateral part of the skull,[12] thus becoming impracticable for application in neurosurgery experiments[11] and chronic postoperative management. The sheep skull bone anatomy is distinguished by less skull cap convexity than human and primates,[33] requiring a bespoke head frame design to be used in near investigation studies.

In literature, previous studies[10,11,34] have used an experimental stereotactic frame which is not applicable in a clinical setting because the lack of MRI compatibility involves the use of a specific brain Atlas which could lead to inaccuracy during the surgical procedure, this latter bolstered by the variability within the ovine species. Unfortunately, HFS developed by White et al.[9] for swine models cannot be use for sheep as animal model. The anatomical differences between

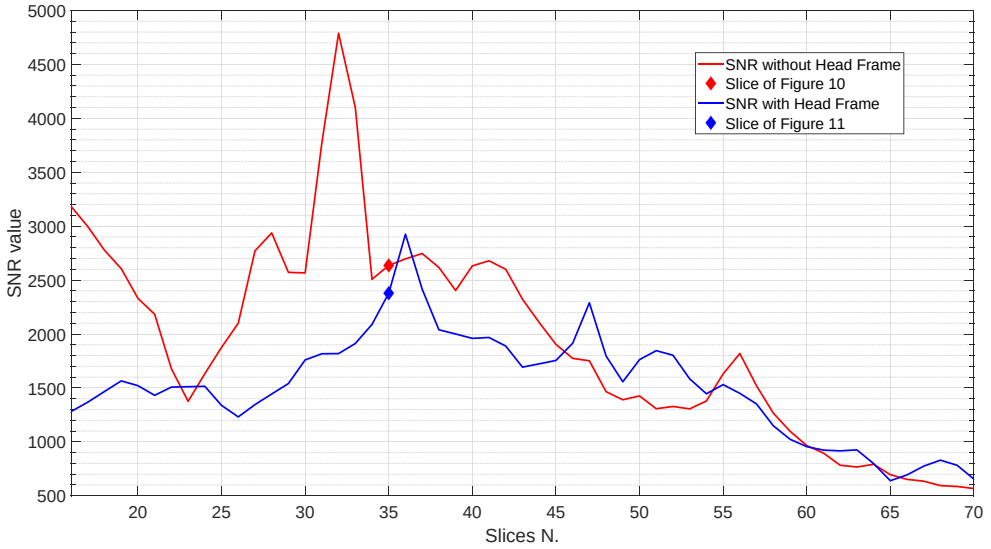

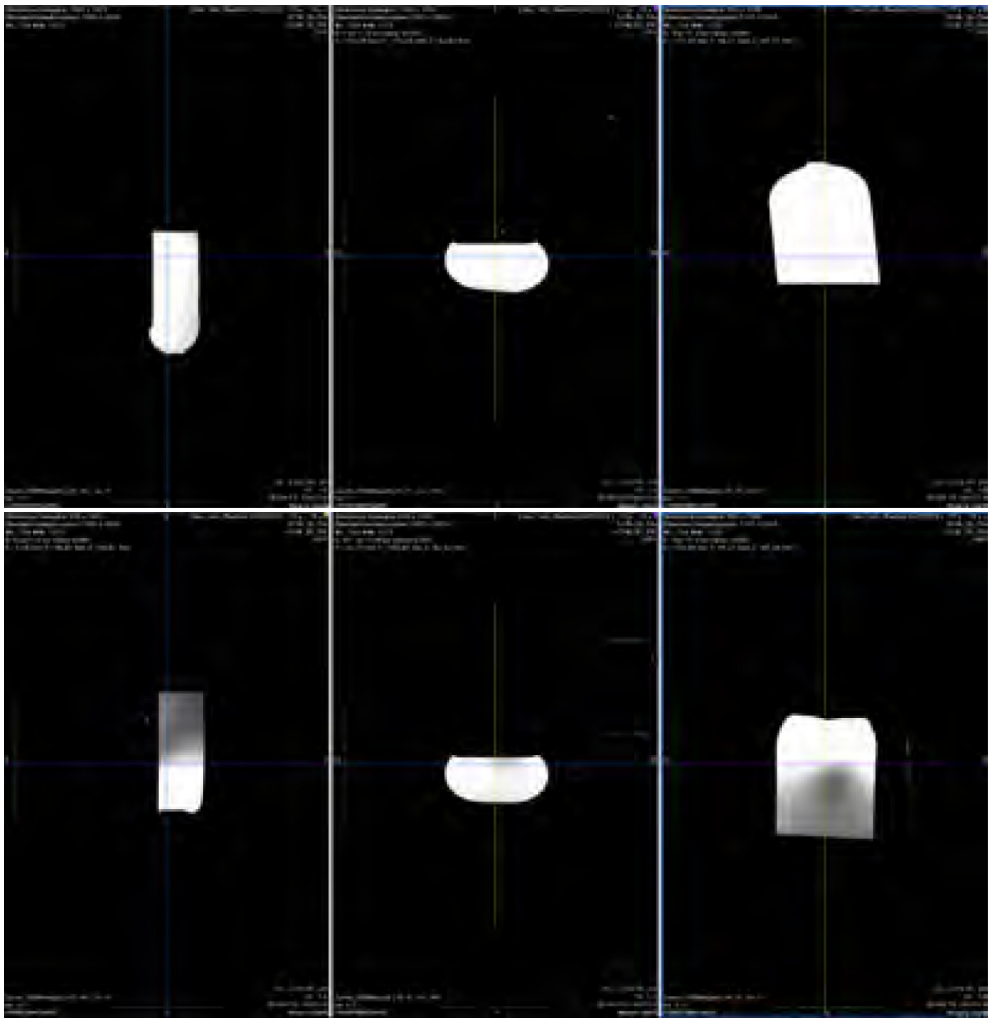

FIGURE 11 Top: SNR for dataset A (red line – without Head Frame) and for dataset B (blue line – with Head Frame). Market points are SNR of the Figures 8 and 9, respectively with value 2636 and 2378 (−9.78%). Middle: MRI sequence with only the phantom (slice n.35). Bottom: MRI sequence with phantom and Head Frame (slice n.35). The image reports a visible attenuation of SNR but without geometrical distortion

the skull conformity and shape, the zygomatic arch process position and relation with the mouth, the mouth dimension itself, are limitations to use a swine HFS in sheep. Pig is characterized by anterior pig head with a plane forehead and vertex that end in a high crest while sheep is characterized by major skull cap convexity. In our HFS, the mouth bar features a nose press (grey top component of Figure 5) designed to improving the head stuck position against the head front lifting and sliding. Sheep due to its ruminant herbivores nature, the dorsal incisors are missing in ovine model, this is a major difference with swine which has the dorsal dentition as consequence of his omnivorous nature. The presence or not of the dorsal dental lines could result into a major sliding movement and the consequent necessity of a mouth bar with or without nose press too.

Frameless stereotactic systems could be employed to overcome the variability issue during the surgical procedure,[35] however, the frame-based technique is still considered the gold-standard for a stereotactic approach to the brain[36] in both research studies and in the human clinical practice.[37] To manage the known limitations of frame-based as compared to frameless technique, such as the frame structure and the compatibility with advanced imaging devices, the frame was designed and tested to properly accommodate the ovine head while granting equivalent accuracy,[38,39] especially in the context of interventional MR studies, which are becoming increasingly needed and reported in translational studies. In addition, framed based systems facilitate animal management during general anaesthesia by supporting the head and keeping it fixed in a fastened position during the surgical procedure and transportation (e.g. between the surgical room and the CT or MRI suite), making a potential displacement during animal management highly unlikely. Such displacement can alter the navigation and stereotactic plan, thus requiring a reset of the procedure. Last, amid frame systems it is possible to avoid using bone fiducials, which in a research situation are employed on the same day of the surgical procedure, with additional stress to the animal.

5 | CONCLUSION

In this work, we present a novel HFS for the ovine model, to address several clinical requirements of translational studies, such as CT/MRI compatibility, compatibility with a conventional human stereotactic CRW frame, robustness during the surgical procedure and robustness against the anatomical variability which is inherent in the sheep model. The system described in this study may benefit future research projects using sheep as an animal model.

ACKNOWLEDGEMENTS

The authors would like to thank Ruan Terblanche and Patrick Moore of Renishaw Plc for their help in the design of the head frame. This project has received funding from the European Union's EU Research and Innovation programme Horizon 2020 under grant agreement no. 688279.

CONFLICT OF INTEREST

The authors declare no potential conflict of interests.

AUTHOR CONTRIBUTIONS

Max Woolley and Dave Johnsons conceived the design and manufacturing of the head frame. Marco Trovatelli, Stefano Brizzola, Davide Danilo Zani designed and performed the experiments in ex-vivo and in vivo. Antonella Castellano and Paola Magili performed the imaging trials and analysis. Riccardo Secoli contributed to the design of the experiment and the data analysis, and he took the lead in writing the article. Marco Riva, Lorenzo Bello and Andrea Falini help in the refinement of the surgical workflow. Ferdinando Rodriguez y Baena supervised the work and contributed to the writing of the article. All authors provided critical feedback and helped shape the research, analysis and manuscript.

DATA AVAILABILITY STATEMENT

The data that support the findings of this study are available from the corresponding author upon reasonable request.

ORCID

Marco Riva https://orcid.org/0000-0003-4643-6451
Riccardo Secoli https://orcid.org/0000-0003-4688-2494

REFERENCES

1. Martini L, Fini M, Giavaresi G, Giardino R. Sheep model in orthopedic research: a literature review. *Comp Med*. 2001;51(4):292-299.
2. Dai J-X, Ma Y-B, Le N-Y, Cao J, Wang Y. Large animal models of traumatic brain injury. *Int J Neurosci*. 2018;128(3):243-254.
3. Karageorgos L, Hein L, Rozaklis T, et al. Glycosphingolipid analysis in a naturally occurring ovine model of acute neuronopathic Gaucher disease. *Neurobiol Dis*. 2016;91:143-154. https://doi.org/10.1016/j.nbd.2016.03.011
4. Reid SJ, Mckean NE, Henty K, et al. Alzheimer's disease markers in the aged sheep (Ovis aries). *Neurobiol Aging*. 2017;58:112-119. https://doi.org/10.1016/j.neurobiolaging.2017.06.020
5. Stypulkowski PH, Stanslaski SR, Jensen RM, Denison TJ, Giftakis JE. Brain stimulation for epilepsy – local and remote modulation of network excitability. *Brain Stimul*. 2014;7(3):350-358. https://doi.org/10.1016/j.brs.2014.02.002
6. Stypulkowski PH, Giftakis JE, Billstrom TM. Development of a large animal model for investigation of deep brain stimulation for epilepsy. *Stereotact Funct Neurosurg*. 2011;89:111-122. https://doi.org/10.1159/000323343
7. Stypulkowski PH, Stanslaski SR, Giftakis JE. Modulation of hippocampal activity with fornix deep brain stimulation. *Brain Stimul*. 2017;10(6):1125-1132. https://doi.org/10.1016/j.brs.2017.09.002
8. Bjarkam CR, Cancian G, Glud AN, Ettrup KS, Jørgensen RL, Sørensen J-C. MRI-guided stereotaxic targeting in pigs based on a stereotaxic localizer box fitted with an isocentric frame and use of SurgiPlan computer-planning software. *J Neurosci Methods*. 2009;183(2):119-126. https://doi.org/10.1016/j.jneumeth.2009.06.019
9. White E, Woolley M, Bienemann A, et al. A robust MRI-compatible system to facilitate highly accurate stereotactic administration of therapeutic agents to targets within the brain of a large animal model. *J Neurosci Methods*. 2011;195(1):78-87. https://doi.org/10.1016/j.jneumeth.2010.10.023

10. Oheim R, Beil FT, Barvencik F, et al. Targeting the lateral but not the third ventricle induces bone loss in Ewe. *J Trauma Acute Care Surg*. 2012;72(3):720-726.
11. Perentos N, Nicol AU, Martins AQ, Stewart JE, Taylor P, Morton AJ. Techniques for chronic monitoring of brain activity in freely moving sheep using wireless EEG recording. *J Neurosci Methods*. 2017;279:87-100. https://doi.org/10.1016/j.jneumeth.2016.11.010
12. Bjarkam CR, Cancian G, Larsen M, et al. A MRI-compatible stereotaxic localizer box enables high-precision stereotaxic procedures in pigs. *J Neurosci Methods*. 2004;139(2):293-298.
13. Edwards CA, Rusheen AE, Oh Y, et al. A novel re-attachable stereotactic frame for MRI-guided neuronavigation and its validation in a large animal and human cadaver model. *J Neural Eng*. 2018;15(6):066003. https://doi.org/10.1088/1741-2552/aadb49
14. Flecknell P. Replacement, reduction and refinement. *ALTEX*. 2002;19(2):73-78.
15. Pieri V, Trovatelli M, Cadioli M, et al. In vivo diffusion tensor magnetic resonance tractography of the sheep brain: an atlas of the ovine white matter fiber bundles. *Front Vet Sci*. 2019;6:345. https://doi.org/10.3389/fvets.2019.00345
16. Nitzsche Br, Frey S, Collins LD, et al. A stereotaxic, population-averaged T1w ovine brain atlas including cerebral morphology and tissue volumes. *Front Neuroanat*. 2015;9:69. https://doi.org/10.3389/fnana.2015.00069
17. Fedorov A, Beichel R, Kalpathy-Cramer J, et al. 3D slicer as an image computing platform for the quantitative imaging network. *Magn Reson Imaging*. 2012;30(9):1323-1341. Quantitative Imaging in Cancer. https://doi.org/10.1016/j.mri.2012.05.001
18. Fitzpatrick JM, West JB. The distribution of target registration error in rigid-body point-based registration. *IEEE Trans Med Imaging*. 2001;20(9):917-927. https://doi.org/10.1109/42.952729
19. Site VA. *Scanning Instructions for Use of the MR Phantom for the ACRTM MRI Accreditation Program, Reston*. VA: The American College of Radiology; 2020.
20. Rosslyn. Determination of signal-to-noise ratio (SNR) in diagnostic magnetic resonance imaging. *National Electrical Manufacturers Association (NEMA)*. 2008;229(3):215-224.
21. Kaufman L, Kramer DM, Crooks LE, Ortendahl DA. Measuring signal-to-noise ratios in MR imaging. *Radiology*. 1989;173(1):265-267. https://doi.org/10.1148/radiology.173.1.2781018
22. Henkelman RM. Measurement of signal intensities in the presence of noise in MR images. *Med Phys*. 1985;12(2):232-233. https://doi.org/10.1118/1.595711
23. Dietrich O, Raya JG, Reeder SB, Reiser MF, Schoenberg SO. Measurement of signal-to-noise ratios in MR images: influence of multichannel coils, parallel imaging, and reconstruction filters. *J Magn Reson Imaging*. 2007;26(2):375-385. https://doi.org/10.1002/jmri.20969
24. Nestler EJ, Hyman SE. Animal models of neuropsychiatric disorders. *Nat Neurosci*. 2010;13(10):1161-1169.
25. David JL, Christopher CJ, Ian MC, et al. Continual recordings of cardiac sympathetic nerve activity in conscious sheep. *Am J Physiol Heart CircPhysiol*. 2002;282(1):H93-H99.
26. Finnie J. Animal models of traumatic brain injury: a review. *Australian Vet J*. 2001;79(9):628-633. https://doi.org/10.1111/j.1751-0813.2001.tb10785.x
27. Capitanio JP, Emborg ME. Contributions of non-human primates to neuroscience research. *Lancet*. 2008;371(9618):1126-1135. https://doi.org/10.1016/S0140-6736(08)60489-4
28. Grow DA, McCarrey JR, Navara CS. Advantages of nonhuman primates as preclinical models for evaluating stem cell-based therapies for Parkinson's disease. *Stem Cell Res*. 2016;17(2):352-366. https://doi.org/10.1016/j.scr.2016.08.013
29. Lind NM, Moustgaard A, Jelsing J, Vajta G, Cumming P, Hansen AK. The use of pigs in neuroscience: modeling brain disorders. *Neurosci Biobehav Rev*. 2007;31(5):728-751. https://doi.org/10.1016/j.neubiorev.2007.02.003
30. Sauleau P, Lapouble E, Val-Laillet D, Malbert C-H. The pig model in brain imaging and neurosurgery. *Animal*. 2009;3(8):1138-1151. https://doi.org/10.1017/S1751731109004649
31. Jan R. *Surgery of the Brain and Spinal Cord in a Porcine Model*: 165–173. New York, NY: Springer New York; 2016.
32. Taverner MR, Campbell RG, King RH, Johnson RJ. Effects of gender and genotype on the response of growing pigs to exogenous administration of porcine growth hormone1. *J Animal Sci*. 1990;68(9):2674-2681. https://doi.org/10.2527/1990.6892674x
33. Nitzsche B, Henryk B, Donald L, Johannes B, Vilia Z, DA Y. *Focal Cerebral Ischemia by Permanent Middle Cerebral Artery Occlusion in Sheep: Surgical Technique, Clinical Imaging, and Histopathological Results*: 195–225. New York, NY: Springer New York; 2016.
34. Bom vdI, Moser R, Gao G, et al. Finding the striatum in sheep: use of a multi-modal guided approach for convection enhanced delivery. *J Huntingt Dis*. 2013;2(1):41-45. https://doi.org/10.3233/JHD-130053
35. Staudacher A, Oevermann A, Stoffel MH, Gorgas D. Validation of a magnetic resonance imaging guided stereotactic access to the ovine brainstem. *BMC Vet Res*. 2014;10(216). https://doi.org/10.1186/s12917-014-0216-5
36. Kucharczyk W, Bernstein M. Do the benefits of image guidance in neurosurgery justify the costs? From stereotaxy to intraoperative MR\enleadertwodots. *Am J Neuroradiol*. 1997;18(10):1855-1859.
37. Sciortino T, Fernandes B, Conti Nibali M, et al. Frameless stereotactic biopsy for precision neurosurgery: diagnostic value, safety, and accuracy. *Acta Neurochir*. 2019;161(5):967-974. https://doi.org/10.1007/s00701-019-03873-w
38. Dhawan S, He Y, Bartek J, Alattar AA, Chen CC. Comparison of frame-based versus frameless intracranial stereotactic biopsy: systematic review and meta-analysis. *World Neurosurg*. 2019. https://doi.org/10.1016/j.wneu.2019.04.016
39. Smith JS, Quiñones-Hinojosa A, Barbaro NM, McDermott MW. Frame-based stereotactic biopsy remains an important diagnostic tool with distinct advantages over frameless stereotactic biopsy. *J Neurooncol*. 2005;73:173-179. https://doi.org/10.1007/s11060-004-4208-3

How to cite this article: Trovatelli M, Brizzola S, Zani DD, et al. Development and in vivo assessment of a novel MRI-compatible headframe system for the ovine animal model. *Int J Med Robot*. 2021;1–11. https://doi.org/10.1002/rcs.2257